Inorganic Chemistry

Article

pubs.acs.org/IC

Phase Identification and Structure Solution by Three-Dimensional Electron Diffraction Tomography: Gd–Phosphate Nanorods

Arnaud Mayence,[†] Julien R. G. Navarro,[†] Yanhang Ma,[†] Osamu Terasaki,[†,‡] Lennart Bergström,[†] and Peter Oleynikov*[,†]

[†]Arrhenius Laboratory, Department of Materials and Environmental Chemistry, Stockholm University, Stockholm S-106 91, Sweden

[‡]Graduate School of EEWS, KAIST, Daejeong, Republic of Korea

Supporting Information

ABSTRACT: Hydrothermal synthesis of $GdPO_4$ in the presence of poly(methacrylic acid) yields nanorods with a diameter of 15 nm and an aspect ratio of 20. Powder X-ray diffraction patterns showed that the $GdPO_4$ nanorods display peaks characteristics for both monoclinic and hexagonal structures. Three-dimensional electron diffraction tomography (3D EDT) was used to determine the structures *ab initio* on the basis of reciprocal volume reconstruction of electron diffraction data sets collected from single nanorods. The crystal structure of the monoclinic form was shown to be $P2_1/n$, corroborating previous work. We were able to solve the 3D structure of the hexagonal $P6_222$ form, which has not been reported previously. Our work shows that 3D EDT is a powerful method that can be used for solving structures of single nanocrystals.

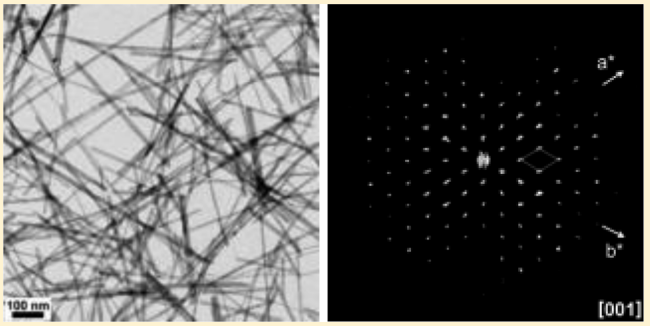

INTRODUCTION

Electron diffraction tomography (EDT) is a general abbreviation for a set of techniques that can be used for structure solution of individual sub-micrometer crystals.[1−4] These methods are based on fast 3D reciprocal space fine scanning which produces high quality 3D data. The collected data sets can be further used for the unit cell determination, quantitative intensities extraction and structure solution. Simultaneously the rough scanning mode followed by the unit cell extraction can be successfully utilized for phase identification. There are two different implementations of the EDT method. One of them is ADT (automated electron diffraction tomography) developed by Ute Kolb[2−4] which is based on acquisition of precession electron diffraction patterns recorded sequentially at a given angular step (usually 1°). ADT method requires a transmission electron microscope (TEM) equipped with any commercially available hardware precession unit. The second method is so-called 3D EDT that has been developed by Peter Oleynikov[1] and utilizes any computer controlled TEM and does not need any extra hardware. This technique combines a mechanical goniometer tilt (large, >2°) with a beam tilt (fine, 0.03−0.1°). Nowadays 3D-EDT data collection has been successfully implemented and tested on variety of JEOL, FEI, and Zeiss electron microscopes. In terms of crystal structure solution both ADT and 3D-EDT methods produce similar results.[1]

Rare earth nanoparticles are interesting candidates in potential biotechnological applications (e.g., fluorescence imaging,[5,6] magnetic resonance imaging[7,8]) and for optical devices.[9,10] Lanthanide orthophosphates besides being chemically stable have a good thermal stability.[11,12] Gadolinium phosphate can be potentially used as a matrix for disposal of nuclear waste.[13−16] It has been also reported as a neutron absorber material suitable for inclusion in spent nuclear fuel canisters.[17] Lanthanide phosphate nanoparticles can be produced through several chemical pathways: solvothermal,[18] hydrothermal,[5] sol–gel process,[19] microemulsion,[20] or spray pyrolysis.[21] Hydrothermal synthesis is attractive because of its low cost and environmentally friendly process that can be easily scaled up.

In this article, we demonstrate that 3D EDT is a powerful technique for nanocrystalline phase identification and further structure determination especially in the case of a mixed phase powder. $GdPO_4$ nanorods were synthesized using an organic polymer, poly(methacrylic acid) (PMAA), under hydrothermal condition. The nanocrystal structures and morphologies were characterized by TEM. Powder X-ray diffraction (PXRD) pattern of the purified product revealed a dimorphic form. An attempt of solving both structures using XRD data failed. Therefore, the crystal structures of each type were individually identified and solved using 3D EDT. The use of this technique permitted us to significantly reduce the TEM work time when compared to the conventional approach that involves manually locating and acquiring electron diffraction patterns from different crystallographic zone axes of a crystal (or several crystals). The structures reported in this work were identified

Received: January 16, 2014
Published: April 25, 2014

 © 2014 American Chemical Society dx.doi.org/10.1021/ic500056r | *Inorg. Chem.* 2014, 53, 5067−5072

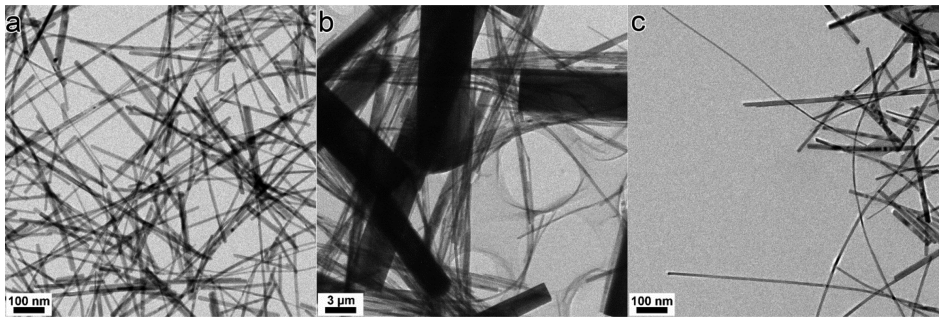

Figure 1. TEM pictures of the as-prepared $GdPO_4$ nanorods synthesized under hydrothermal condition at 180 °C (a) with or (b) without poly(methacrylic acid). (c) Thin nanorods synthesized with PMAA can be both straight and slightly bent.

and solved within a single day. The advantage of 3D EDT is that the investigated crystal does not need to be oriented in advance. Moreover during most of the data collection time the crystal is not aligned along any low-index zone axes. This reduces the dynamical scattering effects significantly. The data completeness depends on the symmetry.[22]

Complementary investigations were carried out *in situ* using variable temperature XRD in order to find out the temperature of the hexagonal form to monoclinic transformation.

EXPERIMENTAL SECTION

Materials. Gadolinium(III) nitrate hexahydrate ($Gd(NO_3)_3{\cdot}6H_2O$, 99.9%) and ammonium phosphate monobasic ($NH_4H_2PO_4$, ≥98%) were purchased from Sigma-Aldrich and used as received. Poly(methacrylic acid) (M_n 100 000) was provided by Polyscience (00578). All the synthesis and surface modification were performed in Milli-Q water.

Synthesis of $GdPO_4$ Nanorods. Hydrothermal synthesis was employed to obtain $GdPO_4$ nanorods. A modified procedure previously described was used.[23] In a typical synthesis, a solution of poly(methacrylic acid) (75 mg, 5 mL) was added, drop by drop, under vigorous stirring to a solution of $Gd(NO_3)_3{\cdot}0.6H_2O$ (5 mL, 50 mg). Then, a solution of ammonium phosphate monobasic solution (5 mL, 32 mg) was added under stirring. The final solution was stirred for 2 min, transferred into a Teflon lined stainless steel autoclave, and heated at 180 °C for 18 h. The final product was then purified by centrifugation (6000 rpm/15 min). The supernatant was slowly discarded, and the rods, present in the bottom, were resuspended in Milli-Q water. This operation was repeated 3 times.

X-ray Diffraction Analyses. Powder X-ray diffraction (PXRD) patterns were collected on a PANalytical X'Pert Pro using Cu Kα1 radiation (45 kV, 40 mA), irradiated length 10 mm, mask fixed 10 mm, and a step size of 0.13° in the Bragg–Brentano configuration. *In situ* investigation was performed on a PANalytical X'Pert Pro in Bragg–Brentano configuration using Cu Kα radiation (45 kV, 40 mA). Temperature elevation was controlled by an Anton Paar TCU 750 control unit. Sample was mounted on a XRK 900 reactor chamber onto a gold thin plate.

TEM and 3D EDT Analyses. TEM measurement were carried out using a JEOL JEM-2100 microscope equipped with LaB_6 filament operated at 200 kV (C_s = 1.4 mm, C_c = 1.8 mm, point resolution = 2.5 Å). In order to obtain quantitative intensities that could be further used for 3D crystal structural solution we have utilized the 3D EDT technique. Three dimensional data was acquired using Analitex EDT-COLLECT software package.[1] During the data collection a set of unique electron diffraction patterns was recorded using electronic beam tilt in the range of ±1.5° (0.15° step) followed by the mechanical goniometer tilt (~3° in our setup). We used an ultrahigh tilt tomography specimen holder which allowed us to scan ~280° of reciprocal space (~140° of the total goniometer tilt in the range from −73° to +65.9°). The whole 3D EDT data set had 1000 unique electron diffraction frames; the total data collection time was 53 min. The 3D EDT data collection was carried out in the nanobeam (NBD) mode using a 50 μm condenser aperture. The illumination area was ~300 nm with the nanorod fully covered by the beam. The CCD camera used was a Gatan ES500W Erlangshen (12 bit, 1350 × 1040). The 3D unit cell determination, the quantitative intensities extraction and the reciprocal volume reconstruction from a set of individual electron diffraction patterns were performed using Analitex EDT-PROCESS software package.[1]

RESULTS AND DISCUSSION

Inorganic Synthesis and Characterization of $GdPO_4$ Nanorods. $GdPO_4$ nanorods were synthesized using hydrothermal process in the presence of poly(methacrylic acid) (PMAA). TEM images of the synthesized nanocrystals with (Figure 1b) and without (Figure 1a) PMAA revealed a substantial difference in their width distribution. The addition of PMAA promotes a narrow width distribution of the nanorods. The average length and width are 300 nm and ~15 nm, respectively (Figure 1a). In comparison, the rods width obtained without polymer varies from 200 nm to 5 μm (Figure 1c). Nanorods having low width-length ratio are most often bent as shown in Figure 1d. The high dose electron exposure may induce bending of some thin nanorods (nanowires).

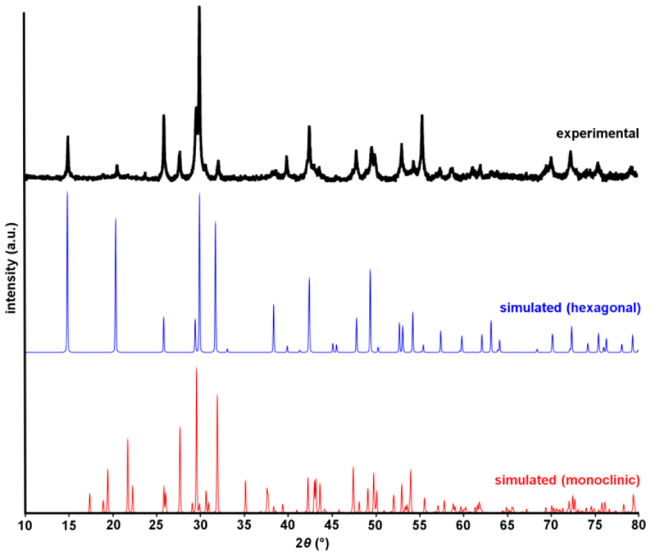

Figure 2. (Top) Experimental PXRD pattern of a dimorphic $GdPO_4$ powder synthesized with PMAA and (middle and bottom) simulated PXRD patterns of both hexagonal and monoclinic forms.

The nanorods capped with PMAA were characterized by Fourier transform infrared (FTIR) spectroscopy revealing the

dx.doi.org/10.1021/ic500056r | Inorg. Chem. 2014, 53, 5067−5072

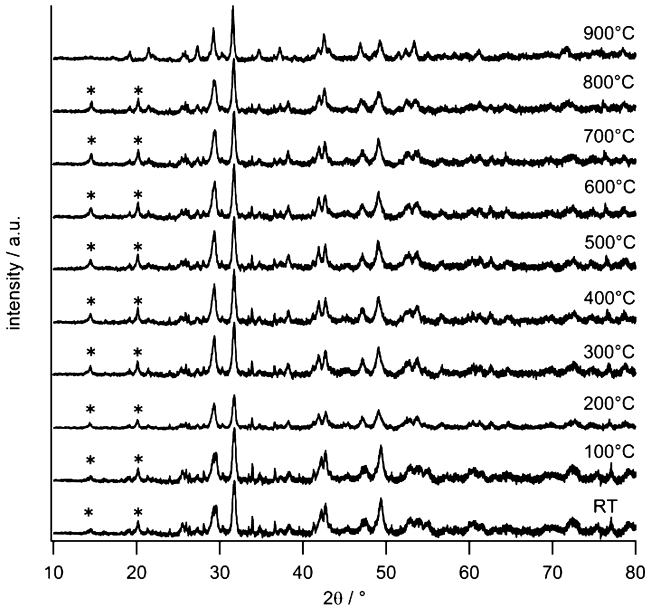

Figure 3. PXRD patterns of the $GdPO_4$ powder at different heating temperatures. The peaks marked with stars depict the hexagonal form present in the powder.

spectral signature of the carboxylic acid (e.g., C═O, 1691 cm^{-1}; O—H, 3510 cm^{-1}). Moreover, the zeta potential measurements show that the nanorods are negatively charged in the pH range 3−10, confirming the poly acid adsorption on the rods surface (see Supporting Information).

X-ray Diffraction Analyses. The precipitated and purified powder of $GdPO_4$ nanorods was characterized by powder X-ray diffraction (PXRD) as a mixture of a hexagonal form (ICDD 39-0232) and a monazite-type compound which crystallizes as a monoclinic form (ICDD 32-0386) (Figure 2).

Two structures that are commonly observed for rare earth orthophosphates are the monazite[25] ($P2_1/n$, monoclinic crystal system) and xenotime (isostructural to the tetragonal zircon type $I4_1/amd$).[26] Nevertheless, the hexagonal form can be obtained under specific synthetical conditions. It was noticed that experimental conditions (temperature, precursor type, pH) have a strong influence on the structure type of rare earth orthophosphate obtained.[27,28]

The hexagonal form can be dehydrated and furthermore converted by thermal treatment to the monoclinic form.[29−32] Hikichi et al.[33] highlighted the formation of the gadolinium orthophosphate hexagonal form at low temperature synthesis (20−90 °C).

Mooney[34,35] reported the structures of some rare-earth orthophosphates (La, Ce, Pm, Nd, and Sm). Crystals were found to be dimorphic having monoclinic ($P2_1/n$) and hexagonal structures. The space group derived during the PXRD data analysis of the $CePO_4$ hexagonal form was $P6_222$ (D_6^4) which from the peak position and extinction condition is indistinguishable from $P3_121$ (D_3^4) taking only powder data into account. These space groups were inferred on the basis of the assumption that the structural arrangement of phosphate ions is similar to that of KH_2PO_4. A few years later, Hezel and Ross[29,36] confirmed the existence of a hexagonal form for the lanthanide series of elements from lanthanum to dysprosium (La,Ce, Pr, Nd, Pm, Sm, Eu, Gd, Dy). IR spectrum analysis revealed that the oxygen occupancy in phosphate groups is consistent with $P3_121$ space group. XRD data on powder from this study is listed in the PDF database as ICDD 39-0232. Subsequent investigations concluded that the hexagonal form could be assigned to be $P3_121$, but another opted for $P6_222$.[37−39] So far, there is no single crystal X-ray data available for the hexagonal form. This might be due to some practical difficulties encountered in the synthesis and the isolation of a single hexagonal lanthanide orthophosphate crystal. Hence, despite the large number of investigations and publications on rare earth orthophosphates, the space group assignment for the hexagonal form is still unclear, and its structure solution was never obtained.

The transformation of hexagonal $GdPO_4$ nanorods into monoclinic lattice was followed by *in situ* variable temperature X-ray diffraction analysis under vacuum ∼1 mbar (Figure 3). The sample was heated continuously at a rate of 20 °C min^{-1} up to 900 °C. The temperature of the sample was kept constant during data acquisition. The complete conversion of the hexagonal into the monoclinic form occurs above 800 °C. The XRD spectra recorded at 900 °C revealed the absence of the characteristic peaks (indexed with stars) associated with the hexagonal crystal system. These results are consistent with previous studies on the stability and transformation of the hexagonal form.[31,40]

Electron Diffraction Tomography (3D EDT). The 3D electron diffraction tomography method can overcome problems encountered in the powder X-ray diffraction technique. The main advantage is that we can collect 3D data from almost any individual nanocrystal in the powder. In this case, we could uniquely identify and perform full characterization of different crystal types in the mixed powder sample. The phase identification procedure involves only a rapid scan (0.5° beam tilt steps) of individual crystals in order to extract the unit cell information and possible extinction conditions.

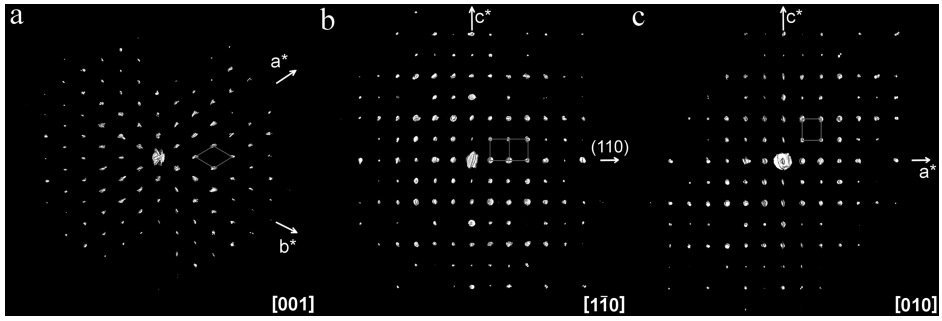

Figure 4. Projections of reconstructed reciprocal space volume of an individual hexagonal $GdPO_4$ nanorod along (a) [001], (b) [1−10], and (c) [010] zone axes.

dx.doi.org/10.1021/ic500056r | *Inorg. Chem.* 2014, 53, 5067−5072

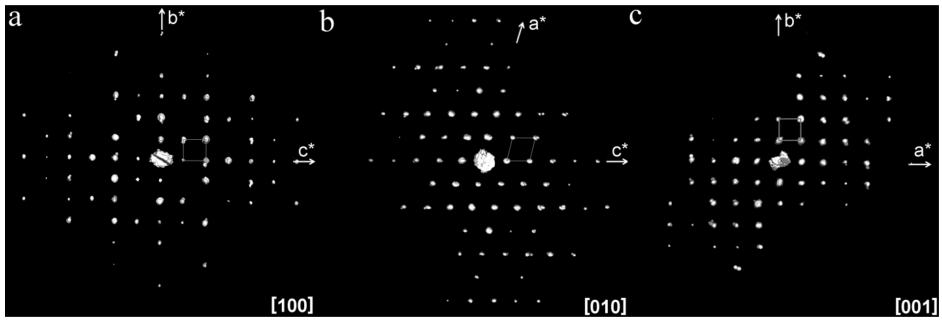

Figure 5. Three projections of the reconstructed reciprocal space volume of the $GdPO_4$ monoclinic form along (a) [100], (b) [010], and (c) [001] zone axes.

Table 1. Experimental Parameters and Details of the Data Set for the $GdPO_4$ Hexagonal Form

Experimental Parameters	
tilt range (deg)	−73.0° to +65.9°
total reflns	791
indep reflns	86
resolution (Å)	0.9
refln coverage (%)	84
R_{sym}	15.3%
R (Sir2011 solution)	6.8%
R1 (Jana2006 refinement)	13.1%
Crystal Data	
chemical formula	$GdPO_4$
M_r	252.2
space group	$P6_222$
a, b, c (Å)	6.9, 6.9, 6.31
V (Å^3)	260.15
Z	12
radiation	electrons, λ = 0.025 08 Å
data collection method	3D EDT, JEOL JEM-2100 LaB_6
absorption correction	none
R_{int}	24.2%
Refinement	
R ($I > 3\sigma(I)$), wR	13.1%, 22.6%
no. of reflns	86
no. of params	7

Table 2. Crystallographic Data for the $GdPO_4$ Hexagonal Form[a]

	x	y	z	U (Å^2)
Gd	0.5	0	0.5	0.022
P	0.5	0	0	0.027
O	0.303	0.860	0.152	0.014

[a]Atomic coordinates and thermal parameters obtained from the refinement (Jana2006).[42].

The reciprocal space coverage in this case can be cut down to 30−50° which depends on the reciprocal lattice: small real-space unit cells would require larger reciprocal space coverage in order to identify the reciprocal vectors correctly. In order to continue with the crystal structure solution, a fine scan of reciprocal space on each individual nanorod can be performed. The phase identification requires less data collection time (15−25 min) than the full scan for the crystal structure solution (45−60 min).

The reconstructed reciprocal space volume from individual electron diffraction patterns of a single $GdPO_4$ nanorod is shown in Figure 4. The unit cell parameters were extracted from this data set, and the hexagonal form was uniquely determined. The calculated crystal orientation matrix revealed that the preferential crystal growth occurs along [001].

Space Group Determination. Reciprocal volume shows only one systematic extinction condition for ($00l$, $l = 3n$) reflections. Using only this observation, it is not possible to distinguish uniquely the space group.[41] The set of accessible space groups is {$P6_222$, $P6_422$}, {$P6_2$, $P6_4$}, {$P3_121$, $P3_221$}, and {$P3_1$, $P3_2$}. The curly brackets combine pairs of enantiomorphic space groups. There are two sets of possible space groups in the following: (a) hexagonal crystal system, $P6_2$, $P6_4$, $P6_222$, and $P6_422$; and (b) trigonal crystal system, $P3_121$, $P3_221$, $P3_1$, and $P3_2$. Each of these space groups was tested during crystal structure solution in Sir2011 program and later refined in JANA2006.[42] The lowest R1 factors in each of the two crystal systems were 13.1% for the hexagonal $P6_222$ space group and 14.7% for the trigonal $P3_121$ space group. The refined lattice parameters from the PXRD data were found to be $a = b =$ 6.9014(2) Å and c = 6.3096(7) Å. The structure solutions in hexagonal ($P6_222$) and trigonal ($P3_221$) space groups produce similar results with a $^1/_3$ relative shift along the c-axis. Currently we cannot distinguish the enantiomorphic space groups due to the experimental conditions. Therefore, we choose the higher

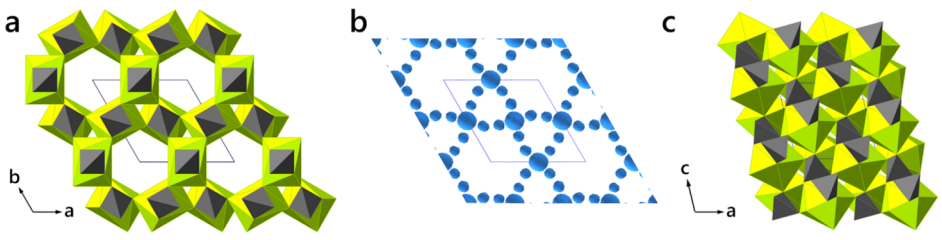

Figure 6. Projections of the hexagonal $GdPO_4$ structure model along [001]: (a) polyhedra−tetrahedra network and (b) the potential map obtained from the direct methods solution using the 3D EDT data set. (c) Projection of the monoclinic $GdPO_4$ structure model along [010].

dx.doi.org/10.1021/ic500056r | Inorg. Chem. 2014, 53, 5067−5072

symmetry $P6_222$ as the actual space group for the $GdPO_4$ hexagonal form.

We were able to locate and identify another nanorod with a monoclinic lattice which corresponds to the monoclinic $P2_1/n$ space group. The reconstructed reciprocal space volume is shown in Figure 5. The systematic extinction conditions found were ($h0l$, $h + l = 2n + 1$) and ($0k0$, $k = 2n + 1$) that uniquely identified the $P2_1/n$ monoclinic space group. The structure solution using our 3D EDT data set is in agreement with previous studies that have reported a monazite type $GdPO_4$.[26,43,44]

Structure Solution of Hexagonal Form. The structure model of the hexagonal $GdPO_4$ was determined *ab initio* using the direct methods on the intensities extracted from the 3D EDT data set. The experimental details are listed in Table 1; the crystallographic data for the hexagonal structure is summarized in Table 2. There were 86 independent reflections used for the structure solution with the final *R*-values R1 = 13.1% and wR2 = 22.6%. Gadolinium atoms are coordinated by eight oxygen atoms where half of them are separated by a distance of 2.28 Å and the rest by 2.59 Å. Phosphorus atoms are surrounded by four oxygen atoms in a tetrahedral arrangement. The P−O bond length is 1.52 Å.

The structure consists of a three-dimensional network of Gd (yellow) and phosphate (gray) polyhedra that are alternately connected forming chains along the *c*-axis (Figure 6a). Polyhedra chains are linked to each other such that channels are created along the *c*-direction allowing water to be accommodated inside the pores. The polyhedral arrangement in the hexagonal form results in a lower density compared to the monoclinic type. Chemically bound water could not be found in the resulting structure. This is probably due to the high vacuum conditions ($\sim 10^{-2}$ mbar) as well as the tendency of the hexagonal form to dehydrate.[31]

CONCLUSIONS

Structure solution of nanocrystals is sometimes not possible to obtain from X-ray powder data especially in the case of a mixture of two or more different phases. The 3D electron diffraction tomography is a very powerful method for (a) the fast phase identification and (b) the crystal structure solution of nanocrystalline samples. This approach allows the collection of 3D diffraction data from individual nanometer-sized crystals. 3D EDT was used to obtain for the first time quantitative single crystal diffraction data from a hexagonal gadolinium orthophosphate form that was used for further *ab initio* crystal structure solution.

ASSOCIATED CONTENT

Supporting Information

IR spectrum and zeta potential of $GdPO_4$ nanorods. Crystallographic information file (CIF) for crystal structure at $T = 295$ K. Animated clip of reciprocal space volume reconstruction of an individual hexagonal $GdPO_4$ nanorod. This material is available free of charge via the Internet at http://pubs.acs.org.

AUTHOR INFORMATION

Corresponding Author

*E-mail: peter.oleynikov@mmk.su.se.

Notes

The authors declare no competing financial interest.

ACKNOWLEDGMENTS

This work was financed by the Swedish Research Council (VR). The Knut and Alice Wallenberg (KAW) Foundation is acknowledged for providing the electron microscopy facilities and financial support (3DEM-NATUR project, A.M. and L.B.). The authors would like to thank Lars Eriksson for the discussion on the space group determination.

REFERENCES

(1) Gemmi, M.; Oleynikov, P. *Z. Kristallogr.* **2013**, *228*, 51−58.
(2) Mugnaioli, E.; Andrusenko, I.; Schüler, T.; Loges, N.; Dinnebier, R. E.; Panthöfer, M.; Tremel, W.; Kolb, U. *Angew. Chem., Int. Ed.* **2012**, *51*, 7041−7045.
(3) Gorelik, T. E.; van de Streek, J.; Kilbinger, A. F. M.; Brunklaus, G.; Kolb, U. *Acta Crystallogr., Sect. B* **2012**, *68*, 171−181.
(4) Andrusenko, I.; Mugnaioli, E.; Gorelik, T. E.; Koll, D.; Panthöfer, M.; Tremel, W.; Kolb, U. *Acta Crystallogr., Sect. B* **2011**, *67*, 218−225.
(5) Ren, W.; Tian, G.; Zhou, L.; Yin, W.; Yan, L.; Jin, S.; Zu, Y.; Li, S.; Gu, Z.; Zhao, Y. *Nanoscale* **2012**, *4*, 3754−3760.
(6) Rodriguez-Liviano, S.; Becerro, A. I.; Alcántara, D.; Grazú, V.; de la Fuente, J. M.; Ocaña, M. *Inorg. Chem.* **2013**, *52*, 647−654.
(7) Dumont, M. F.; Baligand, C.; Li, Y.; Knowles, E. S.; Meisel, M. W.; Walter, G. A.; Talham, D. R. *Bioconjugate Chem.* **2012**, *23*, 951−957.
(8) Hifumi, H.; Yamaoka, S.; Tanimoto, A.; Akatsu, T.; Shindo, Y.; Honda, A.; Citterio, D.; Oka, K.; Kuribayashi, S.; Suzuki, K. *J. Mater. Chem.* **2009**, *19*, 6393−6399.
(9) Chaput, F.; Lerouge, F.; Tusseau-Nenez, S.; Coulon, P.-E.; Dujardin, C.; Denis-Quanquin, S.; Mpambani, F.; Parola, S. *Langmuir* **2011**, *27*, 5555−5561.
(10) Moretti, F.; Vedda, A.; Nikl, M.; Nitsch, K. *J. Phys.: Condens. Matter* **2009**, *21*, 155103.
(11) Schlenz, H.; Heuser, J.; Neumann, A.; Schmitz, S.; Bosbach, D. *Z. Kristallogr.* **2013**, *228*, 113−123.
(12) Clavier, N.; Dacheux, N.; Podor, R. *Inorg. Chem.* **2006**, *45*, 220−229.
(13) Terra, O.; Clavier, N.; Dacheux, N.; Podor, R. *New J. Chem.* **2003**, *27*, 957−967.
(14) Boatner, L. A.; Abraham, M. M.; Sales, B. C. *Inorg. Chim. Acta* **1984**, *94*, 146−148.
(15) Ewing, R. C.; Weber, W. J.; Clinard, F. W. *Prog. Nucl. Energy* **1995**, *29*, 63−127.
(16) Pepin, J. G.; Vance, E. R.; Mccarthy, G. J. *Mater. Res. Bull.* **1981**, *16*, 627−633.
(17) Lessing, P. A.; Erickson, A. W. *J. Eur. Ceram. Soc.* **2003**, *23*, 3049−3057.
(18) Patra, C. R.; Alexandra, G.; Patra, S.; Jacob, D. S.; Gedanken, A.; Landau, A.; Gofer, Y. *New J. Chem.* **2005**, *29*, 733−739.
(19) Rajesh, K.; Shajesh, P.; Seidel, O.; Mukundan, P.; Warrier, K. G. K. *Adv. Funct. Mater.* **2007**, *17*, 1682−1690.
(20) De Sousa Filho, P. C.; Serra, O. A. *J. Phys. Chem. C* **2011**, *115*, 636−646.
(21) Wuled Lenggoro, I.; Xia, B.; Mizushima, H.; Okuyama, K.; Kijima, N. *Mater. Lett.* **2001**, *50*, 92−96.
(22) Mugnaioli, E.; Kolb, U. *Microporous Mesoporous Mater.* **2013**, *166*, 93−101.
(23) Fang, Y.-P.; Xu, A.-W.; Song, R.-Q.; Zhang, H.-X.; You, L.-P.; Yu, J. C.; Liu, H.-Q. *J. Am. Chem. Soc.* **2003**, *125*, 16025−16034.
(24) Burla, M. C.; Caliandro, R.; Camalli, M.; Carrozzini, B.; Cascarano, G. L.; Giacovazzo, C.; Mallamo, M.; Mazzone, A.; Polidori, G.; Spagna, R. *J. Appl. Crystallogr.* **2012**, *45*, 357−361.
(25) Clavier, N.; Podor, R.; Dacheux, N. *J. Eur. Ceram. Soc.* **2011**, *31*, 941−976.
(26) Ni, Y.; Hughes, J. M.; Mariano, A. N. *Am. Mineral.* **1995**, *80*, 21−26.
(27) Kolitsch, U.; Holtstam, D. *Eur. J. Mineral.* **2004**, *16*, 117−126.
(28) Du Fou de Kerdaniel, E.; Clavier, N.; Dacheux, N.; Terra, O.; Podor, R. *J. Nucl. Mater.* **2007**, *362*, 451−458.

(29) Hezel, A.; Ross, S. D. *J. Inorg. Nucl. Chem.* **1967**, *29*, 2085−2089.
(30) Assaaoudi, H.; Ennaciri, A.; Rulmont, A.; Harcharras, M. *Phase Transitions* **2000**, *72*, 1−13.
(31) Jonasson, R. G.; Vance, E. R. *Thermochim. Acta* **1986**, *108*, 65−72.
(32) Glorieux, B.; Matecki, M.; Fayon, F.; Coutures, J. .; Palau, S.; Douy, A.; Peraudeau, G. *J. Nucl. Mater.* **2004**, *326*, 156−162.
(33) Hikichi, Y.; Sasaki, T.; Suzuki, S.; Murayama, K.; Miyamoto, M. *J. Am. Ceram. Soc.* **1988**, *71*, C−354−C−355.
(34) Mooney, R. C. L. *J. Chem. Phys.* **1948**, *16*, 1003.
(35) Mooney, R. C. L. *Acta Crystallogr.* **1950**, *3*, 337−340.
(36) Hezel, A.; Ross, S. D. *Spectrochim. Acta* **1966**, *22*, 1949−1961.
(37) Steger, E.; Schmidt, W. *Ber. Bunsen-Ges.* **1964**, *68*, 102−109.
(38) Assaaoudi, H.; Ennaciri, A.; Rulmont, A. *Vib. Spectrosc.* **2001**, *25*, 81−90.
(39) Wegel, F.; Scherrer, V.; Henschenl, H. *Radiochim. Acta* **1965**, *4*, 18−23.
(40) Hikichi, Y.; Hukuo, K. I.; Shiokawa, J. *Bull. Chem. Soc. Jpn.* **1978**, *51*, 3645−3646.
(41) Hahn, T. *International Tables for Crystallography*; Springer: New York, 2005.
(42) Petricek, V.; Dusek, M.; Palatinus, L. *JANA2006. The Crystallographic Computing System*; Institute of Physics: Praha, Czech Republic, 2006.
(43) Mullica, D. F.; Grossie, D. A.; Boatner, L. A. *Inorg. Chim. Acta* **1985**, *109*, 105−110.
(44) Weigel, V.; Scherer, V.; Henschel, H. *J. Am. Ceram. Soc.* **1965**, *48*, 383−384.